Formation of Oriented Elliptic Rydberg Atoms

J. C. Day,* T. Ehrenreich, S. B. Hansen, E. Horsdal-Pedersen, K. S. Mogensen, and K. Taulbjerg
Institute of Physics and Astronomy, Aarhus University, DK-8000 Aarhus C, Denmark
(Received 5 October 1993; revised manuscript received 4 January 1994)

Oriented elliptic Rydberg atoms have been formed in a thermal beam of Li atoms by the adiabatic crossed-field method. All coherent elliptic quantum states from linear to circular can be produced by this method. The orientation and eccentricity is controlled by the external fields. While the formation of circular states by the crossed-field method has already been established experimentally, the radiative decay of the Rydberg atoms formed here was measured and compared with theory to verify that highly eccentric elliptic quantum states may also be formed.

PACS numbers: 31.50.+w, 34.60.+z, 34.70.+e

Following a suggestion by Delande and Gay [1] it was recently demonstrated by Hare, Gross, and Goy [2] that oriented circular Rydberg atoms may be formed by the method of crossed electric and magnetic fields. When applied to thermal Li atoms the method consists of the following steps [2]. First, a linear Stark state with parabolic quantum numbers $(n_1,n_2,m)=(24,0,0)$ is formed by resonant three-photon laser excitation ($2s$-$2p$-$3d$ "linear state") in an external electric field $\mathbf{E}$ which is thereafter turned off adiabatically in the presence of an orthogonal magnetic field $\mathbf{B}$. This is realized by letting the thermal atoms drift into a region where $|\mathbf{E}|=0$ while $\mathbf{B}$ is constant. The mean value, $\langle\mathbf{L}\rangle$, of the orbital angular momentum $\mathbf{L}$ of the circular quantum state resulting from these steps is parallel to the external magnetic field $\mathbf{B}$. The transformation of the Rydberg state from linear to circular proceeds through intermediate elliptic states with $\langle\mathbf{L}\rangle$ parallel to $\mathbf{B}$ and $\langle\mathbf{A}\rangle$ antiparallel to $\mathbf{E}$, where $\mathbf{A}$ is the Runge-Lenz vector [1,3]. If the process is terminated at a finite value of $\mathbf{E}$, the method produces fully oriented elliptic quantum states described by the orientation [4] vectors $\langle\mathbf{L}\rangle$ and $\langle\mathbf{A}\rangle$ which are controlled by the external fields $\mathbf{E}$ and $\mathbf{B}$. These are the so-called coherent states. They form a unique set of quantum states giving the best possible geometrical localization of the wave function on a classical Kepler ellipse [3].

Coherent elliptic quantum states are of considerable potential interest in many fields of atomic physics. Within spectroscopy and atomic structure the interest is associated with the broad range of orbital angular momentum quantum numbers, l, including high l values, represented in an elliptic quantum state [3]. High l values are not easily reached by conventional methods. Within the field of atomic collisions availability of target atoms in elliptic states with continuously variable eccentricity e and direction of orientation vector $\langle\mathbf{L}\rangle$ provides a completely new dimension to the study of collision dynamics. A few theoretical studies exist [5–9], but experimental work [10–13] has been done only for states with low values of l and m except for one experiment with circular Rydberg atoms [14]. An unexpected scaling rule for charge transfer from initial states of large electric dipole moment was recently discovered theoretically [9] but has not yet been confirmed experimentally. Linear or near-linear Rydberg atoms would be ideal for this. Elliptic Rydberg atoms of lower e are attractive for studies of classical aspects of fast atomic collisions [5,6] because of their large spatial dimensions and quasiclassical character.

In the present Letter we describe how the crossed-field method has been applied to form coherent elliptic Rydberg states with principal quantum number $n=25$. The radiative decay of the Rydberg ensemble has been measured by using pulsed laser excitation and observing the attenuation of a selected velocity component of the ensemble over the flight path from excitation to detection by selective field ionization (SFI) [15]. We show that the lifetime of an elliptic state may be calculated on the basis of lifetimes for spherical states [16] and we compare our experimental results with detailed calculations based on these lifetimes. Because of quasidegeneracy of the $m=0$ and $|m|=1$ Stark states of the alkali atoms [17] it was not possible with the presently (or the previously [2]) used techniques to completely avoid populating the $(n_1,n_2,m)=(23,0,\pm1)$ Stark states simultaneously with the (24,0,0) state. The $(23,0,\pm1)$ states are very similar to the (24,0,0) state and during the switching process they go through quasielliptic states into quasicircular states, which are superpositions of states with spherical quantum numbers $(n,l,m)=(25,23,23)$ and (25,24,23). The Rydberg states produced are thus the coherent elliptic states [3] mentioned above and possibly states very similar to those.

The experimental arrangement is shown in Fig. 1. Thermal Li atoms are passed through the center holes of eight electrodes ($E1$–$E8$) which define four regions (I–IV) with homogeneous electric fields. In the first region, I, defined by $E1$–$E4$, the field is 150 V/cm. This field separates the two Stark levels $(n_1,n_2,m)=(24,0,0)$ and $(23,0,\pm1)$ by $\sim$4 GHz, but they appear in the experiment as one level. However, the $(23,0,\pm1)$ level may be partly discriminated against by detuning the third laser (FWHM=6.5 GHz) towards the (24,0,0) level. In practice the laser was detuned $\sim$6 GHz from the peak value. All lasers are linearly polarized parallel to the Stark field E. The laser beams are produced by three dye

0031-9007/94/72(11)/1612(4)$06.00

lasers pumped by a 14 Hz Nd:YAG laser. The next region, II, defined by $E4$ and $E5$ from a transition region in which **E** is 20 V/cm. A fine grid covering the hole in electrode $E4$ ensures homogeneity of the field in the region $E3$ and $E4$ of laser excitation. The Rydberg atoms with $m=0$ are still linear in II, but when passing through electrode $E5$ into region III, they are transformed into elliptic states with orientation vectors $\langle \mathbf{L} \rangle$ and $\langle \mathbf{A} \rangle$ as described above and with eccentricity given by[3]

$$e = 1 \Big/ \left[1 + \left(\frac{2.18}{3n} \frac{B(\mathrm{G})}{E(\mathrm{V/cm})} \right)^2 \right]^{1/2}, \quad (1)$$

where E is the electric field in III and B is a horizontal magnetic field of 0–150 G also present in III. The direction of $\langle \mathbf{L} \rangle$ and the value of e may be varied by adjusting the direction of **B** and the potential V_2 on $E5$, respectively. Earlier experiments [2,14] with targets of Rydberg atoms formed by techniques similar to the present ones show that the target density is high enough for spectroscopic and atomic-collision studies. When the elliptic atoms finally pass through $E8$ into region IV where E is zero, they become circular ($e=0$). The spacing between the electrodes is 5 mm except between $E6$ and $E7$ where it is 10 mm. The distance, L, between the points of laser excitation and field ionization is 50 mm. At about 50 μsec after laser excitation most of the Li atoms have drifted into region IV, and at this time a fast transistor-transistor logic (TTL) pulse (10 V, 5 nsec rise time) is applied to plate TTL and a ramp is started (slew rate 300 V/μsec) on plate high voltage (HV). Ions detected by the secondary electron multiplier after field ionization as the ramp grows form a time spectrum which was recorded by a digital oscilloscope. For **B** parallel to the ramp field the resulting SFI spectrum of circular atoms is nearly identical to the one shown in Fig. 2 of Ref. [14]. It has a main peak and two smaller peaks, one on each side, resulting from near-circular states with $n=24$ and 26. The extracted SFI signal includes the total counts of all three peaks. With this definition of the SFI signal the influence of blackbody radiation [18] from the liquid nitrogen cooled surroundings is effectively reduced. The signal strength, S, is given by

$$S = Kf(v)\left[A_e \exp\left(-\frac{\lambda_l(L_\mathrm{I}+L_\mathrm{II})+\lambda_e L_\mathrm{III}+\lambda_c L_\mathrm{IV}}{L}\Delta t \right) + A_{qe}\exp\left(-\frac{\lambda_{ql}(L_\mathrm{I}+L_\mathrm{II})+\lambda_{qe}L_\mathrm{III}+\lambda_{qc}L_\mathrm{IV}}{L}\Delta t \right)\right], \quad (2)$$

where K is a constant, $f(v)$ is the density of thermal Li atoms with velocity $v=L/\Delta t$ (Δt is the time difference between excitation and field ionization), $L_\mathrm{I}=2.5$ mm is the averaged distance from laser excitation to $E4$, and $L_\mathrm{II}=5$ mm, $L_\mathrm{III}=20$ mm, and $L_\mathrm{IV}=22.5$ mm are the lengths of regions II, III, and IV, respectively. The quantities λ_l, λ_{ql}, λ_e, λ_{qe}, λ_c, and λ_{qc} are decay rates for linear, quasilinear, elliptic, quasielliptic, circular, and quasicircular Rydberg atoms, respectively, and A_e and A_{qe} are the relative populations of the two quasidegenerate Stark levels. The distances depend slightly on the electric field in III. They were found by calculating numerically the field throughout the region covered by the beam and in particular the regions near electrodes $E5$ and $E8$. Before and after the recording of each SFI signal, S, a standard SFI signal, S_N, was taken and used for normalization to eliminate effects on the measurements of unavoidable drifts in laser power, overlap factors, and Li density.

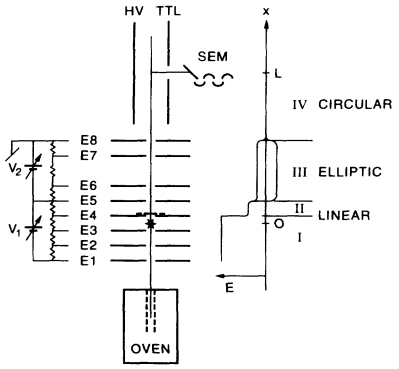

FIG. 1. Experimental setup consisting of an oven for the vertical Li beam, electrodes $E1$–$E8$, voltage supplies V_1 and V_2, lasers producing Rydberg states of Li between $E3$ and $E4$, plates HV and TTL for selective field ionization (SFI), and a secondary electron multiplier (SEM). To the right we show schematically for two values of V_2 the vertical electric field E along the beam axis and identify four regions I–IV in which the Rydberg atoms are linear (I and II), elliptic (III), or circular (IV). A quadrupole magnet (not shown) defines a rotatable, horizontal, homogeneous magnetic field **B** in regions III and IV.

In one type of measurement E/B had the same value in regions II and III and the time interval Δt was varied. The data were normalized to the SFI signal at a small Δt where the signal was strong. The ratio, $R_{e/c}$, between normalized SFI signals for $E/B \neq 0$ and $E/B=0$ corresponding to elliptic and circular states, respectively, has the form of a radiative decay curve. The expression is lengthy in the general case, but it simplifies for $A_e=1$ or $A_{qe}=1$. For $A_e=1$ one finds

$$R_{e/c}(\Delta t) = K_{e/c}\exp\left[-(\lambda_e-\lambda_c)\frac{L_\mathrm{II}+L_\mathrm{III}}{L}\Delta t \right], \quad (3)$$

where $K_{e/c}$ is a constant. In another type of measurement B and E were both zero throughout and the radiative decay of np states was obtained as above by varying Δt. For $A_e=1$, the normalized SFI signal has the form

$$R_{np}(\Delta t) = K_{np}\exp\left[-\left(\lambda_{np} - \lambda_l \frac{L_\mathrm{I}}{L} - \lambda_c \frac{L_\mathrm{II}+L_\mathrm{III}+L_\mathrm{IV}}{L} \right)\Delta t \right], \quad (4)$$

where K_{np} is a constant. In a third and final type of measurement Δt was constant and E was varied to cover e values from zero to almost unity. The data were normalized to the SFI signal for $E=0$. For $A_e=1$, one finds a survival fraction given by

$$R_e(E)=\exp\left[-(\lambda_e-\lambda_c)\frac{L_{III}}{L}\Delta t\right]. \quad (5)$$

The following comparison with theory for elliptic states is based on (3) and (5), while (4) was used to extract experimental decay rates for the p states.

The theoretical decay rate λ_k for an elliptic or quasielliptic state labeled k is given in terms of lifetimes [16] $\tau_{nl}=1/\lambda_{nl}$ for spherical states by

$$\lambda_k=\sum_{l=0}^{n-1}\sum_{m=-l}^{m=l}|a_{lm}^k|^2\lambda_{nl}, \quad (6)$$

where a_{lm}^k are expansion coefficients for the state k on a spherical basis. Although the elliptic state is a coherent superposition of spherical states, there are no interference terms in the total decay rate since such cross terms may be shown to vanish identically in decay processes to isotropic manifolds of final states. In a hydrogenic representation a_{lm}^k may be obtained algebraically [3], but for finite quantum defects an explicit diagonalization of the energy matrix for crossed electric and magnetic fields is necessary. This results in field-dependent a_{lm}^k values and in decay rates which depend not only on E/B (or e) but also weakly on the fields separately. Details of the calculations, which use quantum defects and methods from Ref. [19], and comparison with a broader set of experimental data will be published separately.

The counting errors of the measured SFI signals are generally small and indicated in the figures. Systematic errors come from the ratio E/B (10%) and the lengths L_I-L_{IV} (5%).

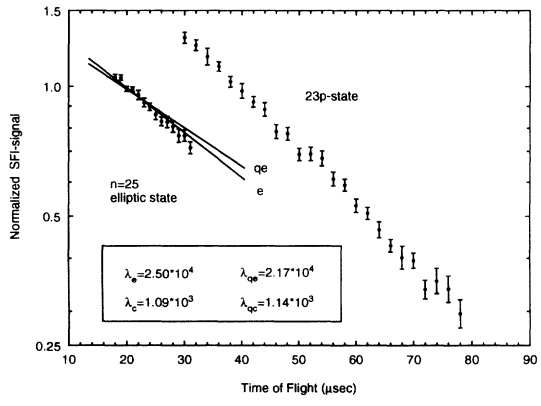

FIG. 2. Radiative decay curves for an elliptic Rydberg state with $n=23$ and $e=0.9987$ ($B=35$ G and $E=20$ V/cm), and for a $23p$ state. The time periods spent in the respective states are shown. Counting errors are indicated by error bars. Theoretical decay rates ($\sec^{-1}$, quantum defects included) used in Eq. (3) are shown. Curve e: $A_e=1$. Curve qe: $A_{qe}=1$.

Experimental and theoretical ratios $R_{e/c}$ are plotted in Fig. 2. The deviation from the theoretical curve for $A_e=1$ is within combined experimental and theoretical errors, but, for $A_{qe}=1$, the agreement is not quite so good, indicating that the quasilinear state is populated only weakly. The experimental technique was checked by measurements of lifetimes for np states with n values from 23 to 26 under field-free conditions. The decay curve for $23p$ is shown in Fig. 2. The np and nf states of Li are both connected with the intermediate $3d$ state by electric dipole transitions and they are separated sufficiently in energy by the quantum defects that selective population of individual np and nf states is possible for a range of n values. The observed decay rates for the f states are much smaller than calculated values. This is due to the almost exact degeneracy of the f state and long lived states of higher l value, which are mixed in by even small stray electric fields. Experimental and theoretical lifetimes for the p states are listed in Table I. The agreement is satisfying.

Experimental and theoretical ratios R_e are plotted in Fig. 3. Negative and positive values of E/B correspond to elliptic states with electric dipole moment parallel and antiparallel to the dipole moment of the initial Stark state, respectively. When plotted vs the experimental parameter E/B, large values of e are accentuated. Results are also plotted directly vs e to show the variation for near circular states. The quantity R_e is independent of the sign of E/B but due to unavoidable and rather stable stray fields (<0.15 V/cm) the symmetry point of the experimental data was not always found at $V_2=0$. Measurements for both positive and negative V_2 are essential for a correct assessment of the zero point for E/B. The symmetry of the experimental data about $E/B=0$ shows that the adiabatic switching works correctly. Two of the theoretical curves shown in Fig. 3 are calculated in a purely hydrogenic basis and show survival fractions for elliptic and quasielliptic states (e-h and qe-h, respectively). Two other curves (e and qe) show results from diagonalizing the energy matrix including crossed electric and magnetic fields and taking into account the quantum defects of s, p, and d states. The hydrogenic description

TABLE I. Lifetimes of Rydberg states. Experimental values for two assumptions on corrections [Eq. (4)]. Statistical standard deviations are indicated. Estimated experimental systematic error 5%. Theory for temperature $T=0$ K. About 10% lower at $T=77$ K.

State	Experiment (μsec)		Theory (μsec)
nl	$A_e=1$	$A_{qe}=1$	$T=0$ K, Ref. [16]
$23p$	30.5 ± 0.6	30.7 ± 0.6	35.2
$24p$	35.5 ± 0.7	35.6 ± 0.7	39.8
$25p$	40.4 ± 1.0	40.6 ± 1.0	44.8
$26p$	46.6 ± 1.7	46.9 ± 1.7	50.2

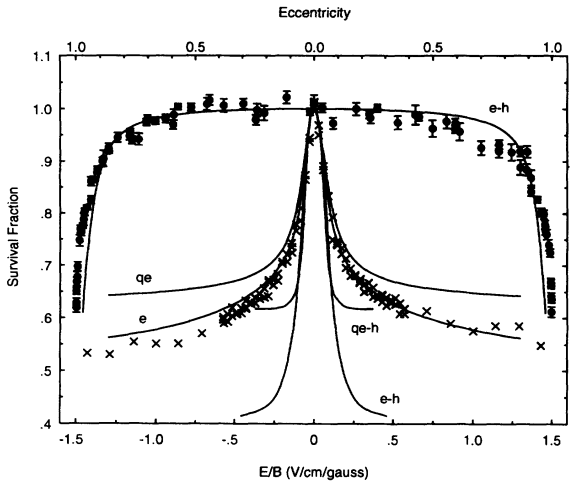

FIG. 3. Experimental and theoretical survival fractions, R_e, of elliptic Rydberg state with $n=25$. Experimental results: Full points, R_e vs eccentricity e as shown on upper scale; crosses, R_e vs E/B as shown on lower scale ($B=50$ G). Theoretical curves [Eqs. (5) and (6)] vs E/B: e-h, hydrogenic for $A_e=1$; qe-h, hydrogenic for $A_{qe}=1$; e, quantum defects included for $A_e=1$; qe, quantum defects included for $A_{qe}=1$. The results labeled e-h are also plotted vs e. The strongly nonlinear relation between E/B and e is revealed by the very different shapes of the two e-h curves.

is accurate in the broad interval $0 \leq e < 0.9$, but for $e > 0.9$ or $E/B > 0.059$ the quantum defects are clearly important. The lifetimes of states with $e < 0.8$ are too long to be measured by the present setup as seen from the near constant value of R_e in this interval. Therefore safe conclusions can be drawn only for $e > 0.8$ or $E/B > 0.039$. The experimental results for this region agree with the theoretical curve (e) for the elliptic states, whereas they deviate somewhat from the curve for quasielliptic states (qe). This is taken as verification that eccentric elliptic states ($e > 0.8$) are indeed formed, with a possible minor contamination by quasielliptic states. SFI spectra for different directions of **B** and previous results [2,14] show that oriented circular atoms are formed in region IV. Since the adiabatic switching takes place at $E5$ between regions II and III, this must be true also in region III when $E/B=0$. For $0 < e < 0.8$ the present data do not offer evidence (except from interpolation) that oriented elliptic states are formed but data to be published on electron capture by 2.5 keV Na^+ ions directed through region III show strong dependence both on e, even for small values of e, and on the direction of **B** supporting our conclusion that also elliptic states with $0 < e < 0.8$ may be formed and controlled.

In conclusion, experimental evidence is presented that the crossed-field method, as expected on theoretical grounds, may be used to produce a target of oriented elliptic Rydberg atoms of sufficient density for spectroscopic and atomic-collision studies to be performed. The eccentricity and the direction of the averaged angular momentum $\langle \mathbf{L} \rangle$ is controlled by external electric and magnetic fields.

We would like to acknowledge advice, discussions, and generous help by K. B. MacAdam, J. L. Sørensen, and E. Wolfrum. The work was supported by the Danish Natural Science Research Council (SNF), the Danish Research Academy, the Carlsberg Foundation (Denmark), and the National Science Foundation under Grant No. INT-9117374.

*Permanent address: Department of Physics and Astronomy, University of Kentucky, Lexington, KY 40506-0055.

[1] D. Delande and J. C. Gay, Europhys. Lett. **5**, 303 (1988).
[2] J. Hare, M. Gross, and P. Goy, Phys. Rev. Lett. **61**, 1938 (1988).
[3] J. C. Gay, D. Delande, and A. Bommier, Phys. Rev. A **39**, 6587 (1989); A. Bommier, D. Delande, and J. C. Gay, *Atoms in Strong Fields*, edited by C. A. Nicolaides *et al.* (Plenum, New York, 1990); C. Lena, D. Delande, and J. C. Gay, Europhys. Lett. **15**, 697 (1991).
[4] U. Fano and J. H. Macek, Rev. Mod. Phys. **45**, 553 (1973).
[5] R. Shakeshaft and L. Spruch, Rev. Mod. Phys. **51**, 369 (1979).
[6] G. A. Kohring, A. E. Wetmore, and R. E. Olson, Phys. Rev. A **28**, 2526 (1983); J. Wang and R. E. Olson, J. Phys. B **26**, L817 (1993).
[7] E. de Prunelé, Phys. Rev. A **31**, 3593 (1985).
[8] T. Yoshizawa and M. Matsuzawa, J. Phys. B **17**, L485 (1984).
[9] J. Macek and S. Y. Ovchinnikov, Phys. Rev. Lett. **69**, 2357 (1992).
[10] K. B. MacAdam, in *Atomic Physics 12*, edited by J. C. Zorn and R. R. Lewis, AIP Conference Proceedings No. 233 (AIP, New York, 1991), p. 310.
[11] P. Roncin, C. Adjouri, M. N. Gaboriaud, L. Guillemot, M. Barat, and N. Andersen, Phys. Rev. Lett. **65**, 3261 (1990); J. C. Houver, D. Dowek, C. Richter, and N. Andersen, Phys. Rev. Lett. **68**, 162 (1992).
[12] F. Aumayr, M. Gieler, J. Schweinzer, H. P. Winter, and J. P. Hansen, Phys. Rev. Lett. **68**, 3277 (1992).
[13] Th. Wörmann, Z. Roller-Lutz, and H. O. Lutz, Phys. Rev. A **47**, R1594 (1993).
[14] S. B. Hansen, T. Ehrenreich, E. Horsdal-Pedersen, K. B. MacAdam, and L. J. Dubé, Phys. Rev. Lett. **71**, 1522 (1993).
[15] R. J. Damburg and V. V. Kolosov, J. Phys. B **12**, 2637 (1979); T. H. Jeys, G. W. Foltz, K. A. Smith, E. J. Beiting, F. G. Kellert, F. B. Dunning, and R. F. Stebbings, Phys. Rev. Lett. **44**, 390 (1980).
[16] C. E. Theodosiou, Phys. Rev. A **30**, 2881 (1984); A. Lindgaard and S. E. Nielsen, At. Data Nucl. Data Tables **19**, 533 (1977). The lifetimes used here are obtained by extrapolation of lifetimes for $n \leq 20$.
[17] C. Fabre, Y. Kaluzny, R. Calabrese, Liang Jun, P. Goy, and S. Haroche, J. Phys. B **17**, 3217 (1984).
[18] W. P. Spencer, A. G. Vaidyanathan, D. Kleppner, and T. W. Ducas, Phys. Rev. A **24**, 2513 (1981).
[19] M. L. Zimmerman, M. G. Littman, M. M. Kash, and D. Kleppner, Phys. Rev. A **20**, 2251 (1979).